RSC Advances

PAPER

View Article Online
View Journal | View Issue

Cite this: *RSC Adv.*, 2020, **10**, 38788

Microstructure control of the wettability and adhesion of Al alloy surfaces

Yonghua Wang,[ab] Zhilei Qin,[a] Jinkai Xu[a] and Huadong Yu *[a]

This article provides a simple and fast method to adjust the wettability and adhesion of aluminum (Al) alloy surfaces after electric discharge machining (EDM). For an Al alloy plate after EDM, without any grinding and polishing, laser treatment was directly performed on the surface to prepare the Al alloy surface with different wettability and adhesion behaviors. Scanning electron microscopy was used to analyze the surface morphologies of the smooth surface, wire-cut surface, and the surface treated with different laser parameters after wire-cut. Then, the chemical composition, contact angle (CA) stability, adhesion and surface bounce behavior of the surfaces processed *via* different treatment steps were tested and analyzed. The results indicated that the crater structure was distributed randomly on the EDM-processed surface, with a static CA of 129 ± 1.2°. After laser engraving, the surface generates a regular arrangement of micron-level grooves/pits. Meanwhile, the molten Al alloy spattered at high temperatures and instantly solidified to produce sub-micron-sized metal particles attached to the pit/bottom of the trench and the unprocessed area, naturally forming a dual-scale structure. This naturally formed dual-scale structure makes the surface static CA up to 154.6 ± 1.2°. This technology realized that only laser treatment is used to control the wettability and adhesion of the Al alloy surface after EDM treatment and expected to provide a simple and low-cost method for the practical application of large-area superhydrophobic surfaces.

Received 15th September 2020
Accepted 28th September 2020

DOI: 10.1039/d0ra07892a

rsc.li/rsc-advances

1 Introduction

Wettability is one of the most important properties to describe solid surfaces, and the wettability of solid surfaces refers to the diffusion capacity of droplets on solid surfaces, generally determined by measuring the CA of water droplets on solid surfaces. Superhydrophobic surfaces were first observed in the natural environment, such as lotus leaves,[1,2] rose petals,[3,4] butterfly wings,[5,6] rice leaves,[7,8] leech legs,[9,10] cicada wings,[11,12] moth wings,[13,14] gecko feet,[15,16] and bird wings.[17] The magical effects of superhydrophobic surfaces in the nature have gained great interest of many researchers, and with the development of technology, these functions of superhydrophobic surfaces have been gradually applied in a number of fields including surface self-cleaning,[18,19] anti-icing,[20,21] corrosion resistance,[22,23] anti-fog,[24] drag reduction,[25,26] oil–water separation,[27–29] and biomedicine.[30,31]

At present, numerous artificial superhydrophobic surfaces are developed. The preparation methods include interference lithography,[32,33] electroplating,[34] solution immersion,[35] sol–gel method,[36,37] chemical/electrochemical engraving erosion,[38,39] and template method.[40] By using the above-mentioned methods, the epidermis of animals and plants was mimicked to create micro/nano-level structures on solid surfaces to solve the practical problems. However, most of these preparation methods have disadvantages such as expensive processing equipment, harsh test conditions, high manufacturing costs, low surface energy material modification, and difficulty in mass production, so that superhydrophobic surfaces cannot be widely used in production and life. At the same time, the use of secondary chemical substance modification not only increases the preparation cost of the superhydrophobic metal surface, but also affects the service life and stability of the metal surface.[41]

Today, using a laser to construct a micro-scale structure on a solid metal surface is a commonly used method, and this micro-scale structure on a metal surface does not collapse or deteriorate over time, which has potentially huge benefits. Zhong *et al.*[42] prepared a superhydrophobic surface with micro-grooves and micro-hole arrays using a femtosecond laser ablation template technology, exhibiting high transparency and stable mechanical properties. Jagdheesh *et al.*[43] fabricated nanochannels and pillars on the surface of Al alloys by nano-second lasers and found that the laser frequency, power, density and pulse width all significantly affected the newly formed Al oxide surface. Li *et al.*[44] used nanosecond laser to process a micro-pit structure on the surface of the smooth Al alloy and control the wettability and adhesion of the Al alloy surface by

[a]*Ministry of Education Key Laboratory for Cross-Scale Micro and Nano Manufacturing, Changchun University of Science and Technology, Changchun 130022, China. E-mail: yuhuadong@cust.edu.cn*

[b]*Key Laboratory of Bionic Engineering (Ministry of Education), Jilin University, Changchun 130022, China*

changing the pit distance. Because it is difficult to control the surface roughness of a large area polished in practical applications, the cost is high and the process is complicated when used on a large scale, which is also an important reason that there are countless preparation methods but rarely put into practical application on a large scale.

Based on the above research, this paper combines EDM and laser processing technology without polishing and any chemical modification technology. After EDM treatment, the Al alloy surface was processed with micro-nano structures with adjustable wettability and adhesion. According to the results, the super-hydrophobic surface exhibited remarkable stability in the air, and this method is simple, less expensive and suitable for large-scale applications.

2 Materials and methods

2.1 Materials

7075 series Al alloys were used as experimental materials (main elements, wt%: Zn 2.8–3.4, Mg 2.1–2.9, Si 1.7–2.3, Cu 0.5–0.9, Fe 0.6–1.2 and the remaining elements AI), and Al samples were cut on a mid-wire CNC wire cutting machine (HA400U). The reagents used in the test included acetone (≥99.5%), absolute ethanol (≥99.7%) deionized water, hydrochloric acid (36–38%) and sodium hydroxide (≥96.0%). Acetone and absolute ethanol are both of analytical grade. Hydrochloric acid and sodium hydroxide solution were used as analytical reagents for the chemical stability of the sample surface. Deionized water was used for CA measurement.

2.2 Sample preparation

The sample preparation process is shown in Fig. 1. First, a sample with a size of 10 mm × 10 mm × 2 mm was cut using a CNC machine with a middle wire, ultrasonically cleaned with acetone, absolute ethanol and deionized water, and dried under atmospheric conditions. A large number of experiments have proved that the selection of different EDM parameters will greatly affect the surface morphology of the processed sample and then directly affect the wettability and adhesion of the sample surface. The processing parameters selected in this experiment are shown in Table 1.

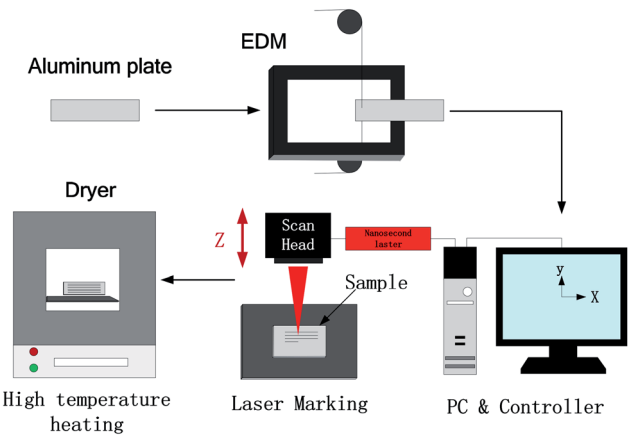

Fig. 1 Schematic of sample preparation.

Table 1 EDM parameters for processing Al alloy surfaces

Wire speed	Current	Pulse width	Interval ratio	Voltage	speed
4 m s^{-1}	2 A	20 μs	6	100 V	7 mm^2 min^{-1}

Then, a laser marking machine was used to write on the sample surface. The wavelength of the laser was 1064 nm, the maximum output power was 20 W, the repetition frequency was 100 Hz, the pulse duration was 100 ns, and the laser spot diameter was 50 μm. The surface was scanned twice at a speed of 1200 mm s^{-1}, and the adjacent line spacing was 10 μm, 50 μm, 100 μm, 150 μm, and 200 μm. The scanning power was 14 W, the frequency was 20 kHz, and a fiber laser marking machine was used. Then, the sample was cleaned ultrasonically using deionized water for 10 minutes. Finally, the sample was taken out and placed into a heater at 200 °C for 1.5 hours.

2.3 Characterization

A scanning electron microscope (SEM, EVO 25, ZEISS) was used to analyze the surface morphology of EDM and laser-processed Al alloys. An energy-dispersive X-ray spectrometer (EDS, X-max) was used to analyze the surface chemical composition of samples by different treatment methods. The CA was measured at room temperature using a CA analyzer (JCJ-001) with 5 μL deionized water. Five different positions were measured on the same surface, and then the average value was taken as the final result to ensure the reliability of the test results. Digital cameras (EOSM3) and ultra-high-speed cameras were used to capture the optical images and bounce behavior of water droplets on the surface (Pco.dimax HS4).

3 Results and discussions

3.1 Morphology

The morphology of the sample was characterized using a scanning electron microscope at a voltage of 20 kV. It can be found in Fig. 2a1 and a2 that the smooth Al alloy surface was very flat, and there were no obvious bumps or depressions on the enlarged surface. After EDM treatment, many crater structures were randomly distributed on the surface, and many bulges around it were surrounded by regular folds (Fig. 2b1 and b2). When EDM was used to process Al samples, spark discharge occurred between the electrode and the processed Al alloy, leading to consumption and corrosion between each other. A small number of materials melted and vaporized on the electrode and the workpiece. In this process, the surface of the workpiece produced a small cavity structure similar to a crescent depression, the size of which depended on the discharge current, pulse width and interval ratio and other different processing and discharge conditions, which eventually led to the formation of a complex crater structure on the sample surface.

Fig. 2c–g shows the microtopography of different multipliers of laser engraving on the surface of the wire cutting–processed

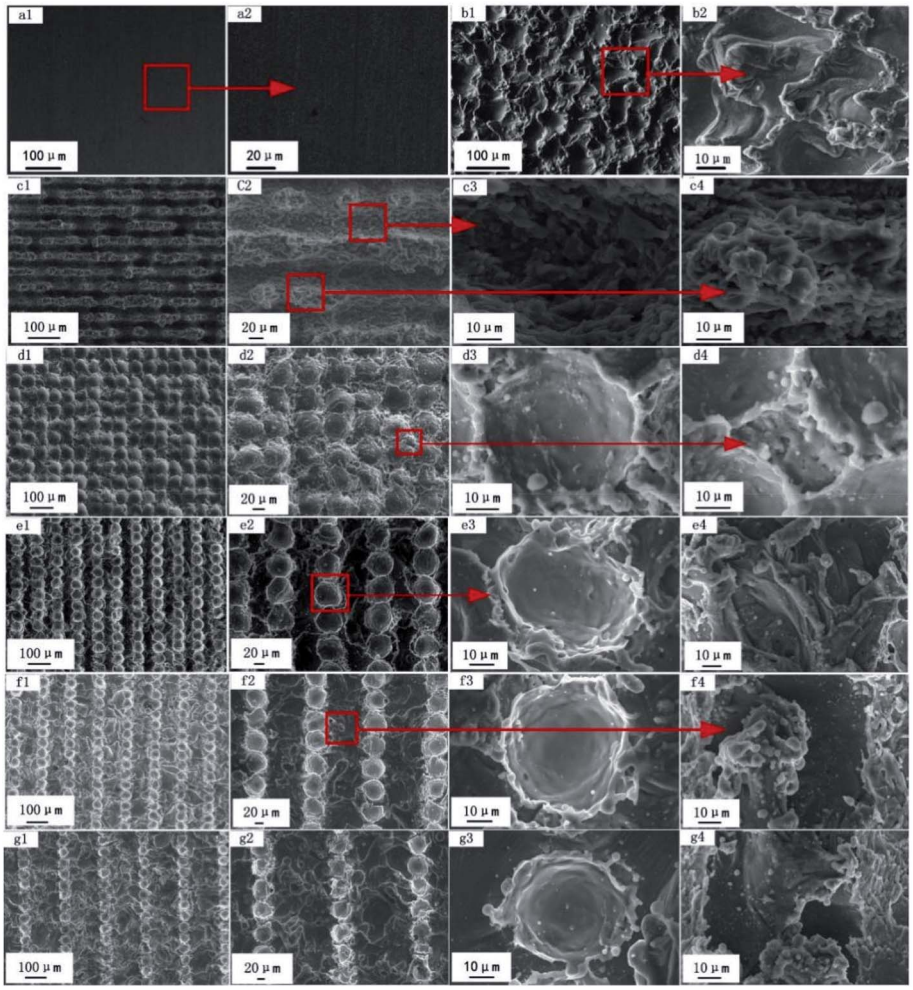

Fig. 2 SEM micrographs of the Al alloy surface: (a1 and a2) smooth Al alloy, (b1 and b2) Al alloy surface morphology after EDM, (c1–g1) marking pitch of 10, 50, 100, 150, and 200 μm low-magnification SEM image, (c2–g2) low-magnification image of pits and untreated area, (c3–g3) high-magnification image of pits and untreated area, (c4–d4) accumulation of the molten Al alloy after laser treatment, and (e4–g4) laser-untreated area.

alloy, and we can see that the surface topography of the sample has also changed with the increase in the laser scan spacing. When the scan spacing was 10 μm, a groove structure was observed in the horizontal direction because the distances between pits were very small, while the molten Al alloy between the grooves was re-stacked into a new raised structure. However, the convex part was not continuous due to EDM (Fig. 2c1 and c2). By further zooming in the grooves and protrusions, it can be found that many sub-micron metal particles were densely distributed on the surface of the micron-sized grooves and the protrusions (Fig. 2c3 and c4). When the scanning distance was 50 μm, the surface of the sample began to change from grooves to closely connected pits (Fig. 2d1 and d2). With the increase in the scanning interval, the EDM area gradually increased (Fig. 2d4–g4). From Fig. 2, we can find that after laser engraving, a regularly arranged groove/pit structure was formed on the surface of the Al alloy. However, due to the irregular crater structure distributed on the surface of the Al alloy after EDM, this structure was destroyed after laser engraving and then distributed in the groove/pit in a fold structure. High-energy irradiation in laser processing made the surface of the Al alloy melt and splash in an instant, and the rapid movement of the laser beam caused the splashed Al alloy particles to cool and cure instantly, and the solidified sub-micron metal particles are distributed on grooves/pits and irregular folds to form a dual-scale structure. The combination of this regular and irregular structure and the naturally formed dual-scale micro-nano structure can easily capture a large amount of air and form an air film on its surface to prevent water flow from penetrating the surface.

3.2 Composition

The second reason for the change in wettability is the change in the chemical composition content of the sample surface after laser processing. Fig. 3 shows the changes in chemical elements on the surface of the EDM-treated Al alloy and the Al alloy at different laser scribing distances compared by energy-dispersive X-ray spectroscopy (EDS). After EDM treatment, the

content of C and O elements on the surface of the sample was greatly increased, while the content of other elements decreased (Fig. 3a). The reason is that the cutting fluid selected in the experiment contained a large amount of grease, and working fluid ionization occurred under the conditions of high temperature and high pressure due to discharge. As a result, carbon and oxygen ions were released, part of which during machining failed to be discharged in time, and generated carbon oxygen compounds sticking to the surface under the combined action of electric field force, beam pressure, high temperature and high pressure, resulting in a significant increase in the content of carbon and oxygen elements.

Fig. 3b–f is the distribution of elements on the surface of the sample after heating when the laser scanning pitch is 10 μm, 50 μm, 100 μm, 150 μm and 200 μm. Laser processing changes the material composition of the sample surface to a certain extent. It can be found that the contents of Zn, Mg and Mn fluctuate slightly after laser processing, while the elements of Al, C and O change greatly. When the laser writing pitch was 10 μm, the C and O content of the sample surface was lower than that of the sample after EDM treatment, while the Al content increased. As the scanning distance increased, the proportion of EDM area gradually increased, and the content of C and O elements began to be improved, when the writing pitch was 200 μm, the proportion of each element on the surface of the sample was close to that of the sample surface after EDM treatment. The high percentage of carbon elements on the surface of the sample can also be attributed to hydrocarbon pollution caused by prolonged exposure to the atmosphere, this surface chemical element change changed the surface-free energy.

3.3 Wettability

Wettability is one of the most important properties to describe the solid surface, and the wettability of the solid surface refers to the diffusion capacity of droplets on the solid surface, generally identified by measuring the CA of water droplets on solid surfaces. Fig. 4 shows the wetting state of the Al alloy surface after EDM treatment and different laser parameter treatments. Ultrasonic cleaning was carried out after EDM treatment, and the cleaned workpiece was placed in an oven at 60–70° for drying for 30 minutes. After drying, the measured surface CA was 129 ± 1.2°, and the water droplets penetrating into the microstructure voids on the Al alloy surface failed to diffuse, maintaining its spherical state.

Fig. 4b–f shows the wetting state of the sample surface subjected to laser processing of the EDM-treated surface, heating at 200 °C for 1.5 hours, and standing in the air for 100 days. We found that the smaller the writing pitch, the greater the change in surface CA as an increase in the number of days of exposure. When the scanning pitch was 10 μm, the sample surface was completely covered with grooves and laser-written stacked microstructures, and droplets penetrated such structures and quickly diffused. The surface still showed super-hydrophilic properties after heat treatment. However, the CA value gradually increased with the increase in the number of days of exposure in the air, and the surface finally demonstrated excellent low viscosity and super-hydrophobicity, indicating that the wetting state was significantly improved.

When the scan line spacing was increased, the exposed EDM area on the sample surface increased, and the sample surface changed from grooves to pits. When the line spacing was 50 μm, the CA was 128 ± 2.1° after heat treatment, and the CA increased to 154.6 ± 1.2° when exposed to air for a period of

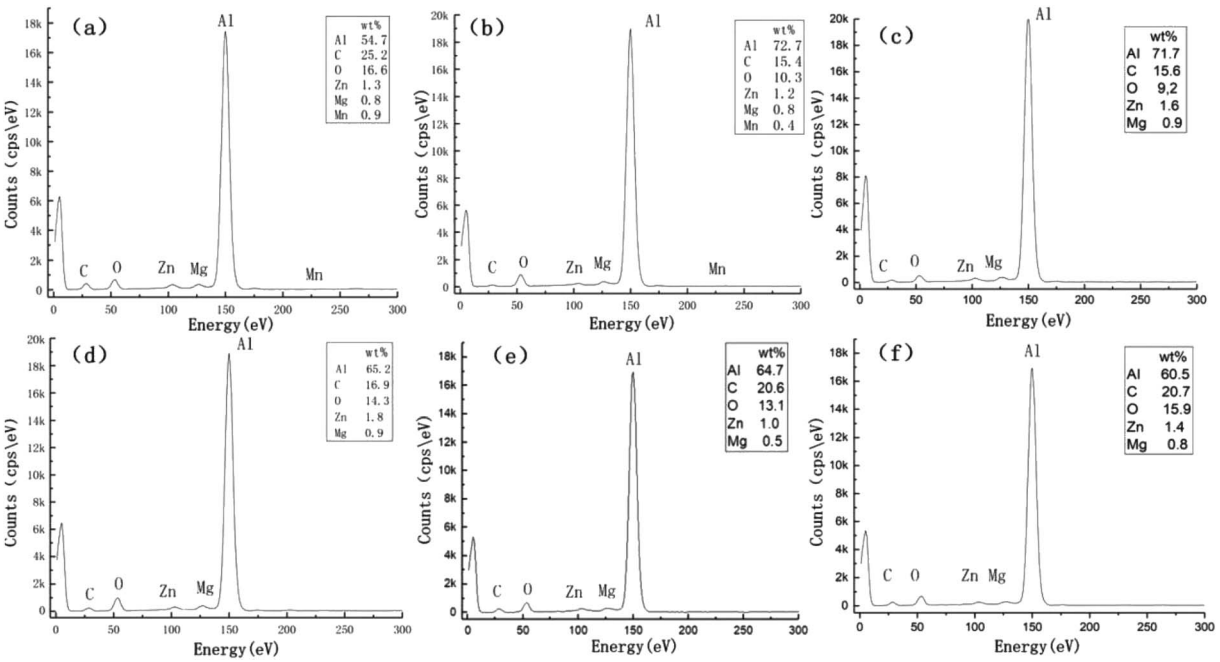

Fig. 3 Al alloy surface elements after laser treatment heating: (a) Al alloy surface elements after EDM, (b) 10 μm, (c) 50 μm, (d) 100 μm, (e) 150 μm, and (f) 200 μm.

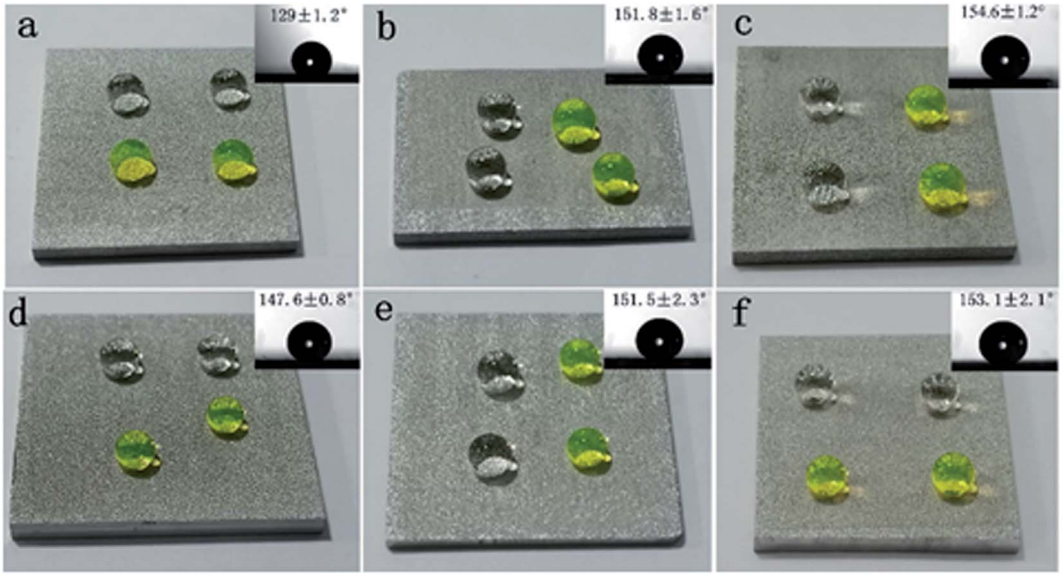

Fig. 4 Sample physical image and the corresponding CA measurement diagram: (a) droplet contact state on the surface after EDM processing, (b–f) the state of water droplet contact on the surface for laser scanning pitch of 10, 50, 100, 150, and 200 μm, respectively. (a–f) The upper right picture is the CA corresponding to the physical picture.

time (Fig. 4c). When the line spacing was 100 μm, 150 μm and 200 μm, the sample showed a high static CA immediately after heating. The surface CA did not change much with time, increasing from 147.1 ± 0.9°, 150.4 ± 1.2° and 152 ± 1.4° to 148.6 ± 1.2°, 151.5 ± 2.3° and 153.2 ± 2.1°, respectively. The high-temperature environment can promote the formation of a passivation layer of Al_2O_3 on the surface of the sample. When it was exposed to the air, a large amount of air resides in the gaps of the micro-nano structure to prevent the penetration of water, so that the water droplets exhibited a high static CA on the surface of the sample.

There are currently two theories (Wenzel model and Cassie–Baxter model) describing the existence of water droplets on a solid surface. The Cassie–Baxter model believes that the presence of a large amount of air in the micro-nano structure gap prevents water from intruding into the gap between them. An intermittent gas–liquid interface is formed between the solid and liquid. Fig. 5 is the three-dimensional morphology of the surface microstructure of the sample after laser processing. When water droplets contact the surface, a large amount of air is trapped in the microstructure voids, causing a small part of the droplets to contact the top of the microstructure but most of the droplets to contact air.

According to the non-smooth surface wettability equation proposed by Cassie and Baxter:

$$\cos\theta = f_1 \cos\theta_1 + f_2 \cos\theta_2 \quad (1)$$

We can calculate the surface area fractions f_1 and f_2 of the Al and air on the composite surface, where θ, θ_1, are the apparent CA and the intrinsic CA of the Al alloy surface (θ_1 is 85 ± 0.9°), θ_2 is the CA of water and air (θ_2 is 180°), and f_1 and f_2 satisfy $f_1 + f_2 = 1$, then the Cassie–Baxter equation can be rewritten as follows:

$$\cos\theta = f_1 \cos\theta_1 - f_2 = \cos\theta_1 - f_2(\cos\theta_1 + 1) \quad (2)$$

Table 2 shows the f_1 and f_2 values calculated according to the equation. The results revealed that the contact area between the water droplets and the solid surface was only about 10%, and most of the water droplet area was in contact with the air trapped in the gap.

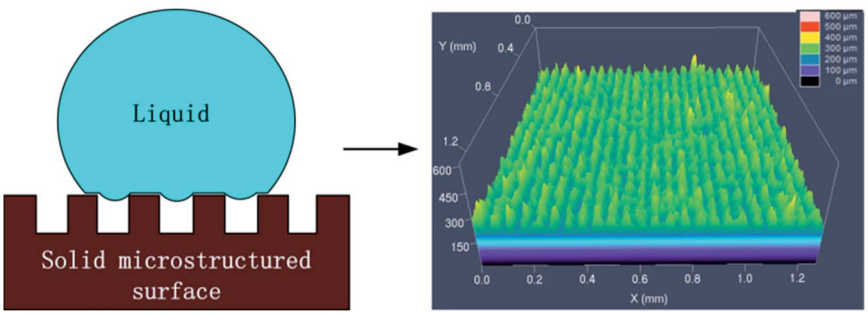

Fig. 5 "Cassie" contact state and three-dimensional topography of the sample surface after laser treatment.

Table 2 The results of f_1 and f_2 based on the Cassie–Baxter equation

Laser engraving line spacing (μm)	CA (°)	f_1	f_2
10	152.5	0.1034	0.8966
50	154.6	0.0885	0.9115
100	148.6	0.1340	0.8660
150	151.5	0.1109	0.8891
200	153.2	0.0983	0.9017

3.4 Adhesivity

The experiment found that the water droplets exhibited different adhesion behaviors on the surface of the sample with different laser marking distances. To describe this feature, we used the pull method and the water drop bounce method for characterization. When a micro-adjustable syringe was used for water drop injection, the adhesion force of the needle is greater than gravity and the water drop hangs on the needle tip. Move the platform slowly upward to bring the sample closer to the water drop. When the water drop contacted the sample surface, it was not adsorbed on the sample surface, it continued to rise, the water droplets on the platform were affected by the supporting force of the sample, and their shape gradually changed from ellipse to spherical and slid upward along the needle (Fig. 6a3–b3). It can be observed that the water droplet slid down the needle and recovered its oval shape under the influence of surface tension after lowering the platform. Continuing to move downwards, the water droplets show an adhesion force by the needle greater than the sum of the adhesion force on the surface of the sample and its own gravity, and finally the droplets separated from the surface of the sample and returned to its original state (Fig. 6a5–b5).

When the writing distance gradually increased, the water droplets exhibited high adhesion on the surface of the sample. The syringe needle was in close contact with the water droplets. Once the suspended droplets contacted the sample surface, they will adhere to the sample surface and no longer separate. With the continuous downward movement of the sample, the water drop was continuously stretched until it was separated from the syringe (Fig. 6c5–e5). After the Al alloy sample was vertically positioned or inverted, the water droplet still adheres tightly to the surface of the sample. The adhesion force was greater than the sum of the gravity of the water droplet and the surface tension between the water droplet molecules. With the increase in scanning distance, a large EDM region existed on the sample surface. Although the rough structure of the sample surface increased the CA, the contact line or contact surface between water droplets and the surface increased due to the water droplets infiltrating into the EDM treatment area, resulting in the high adhesion of water droplets on the sample surface.

In order to observe the dynamic changes in the water droplets on the surface of the sample more clearly, we used an ultra-

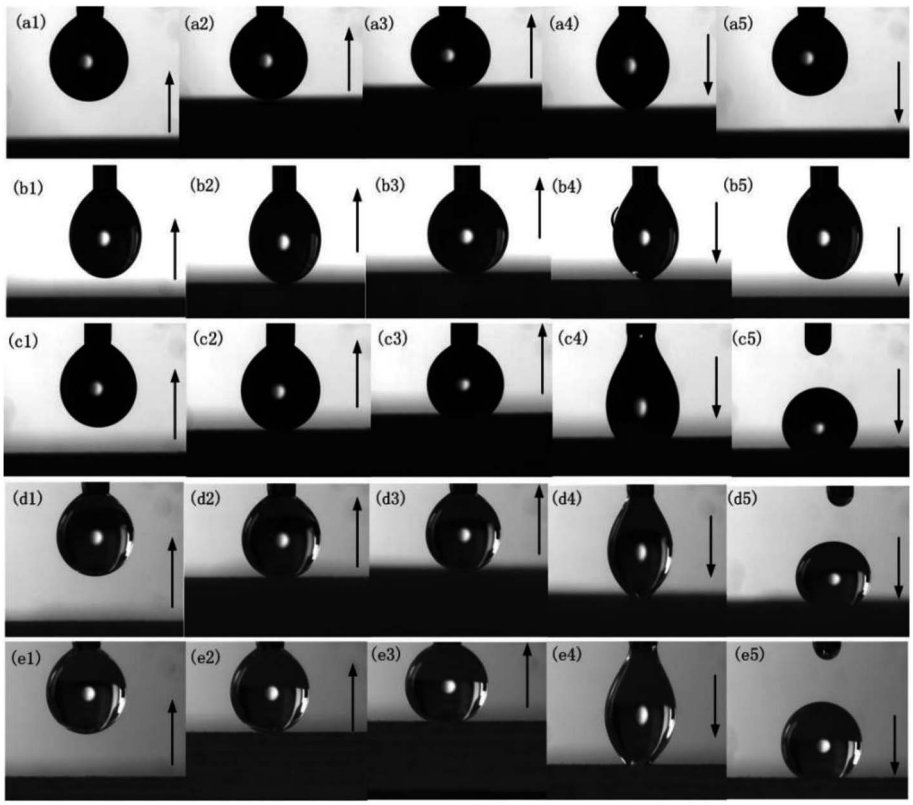

Fig. 6 Dynamic image of droplets contacting the sample surface: (a1–a5) 10 μm, (b1–b5) 50 μm, (c1–c5) 100 μm, (d1–d5) 150 μm, and (e1–e5) 200 μm.

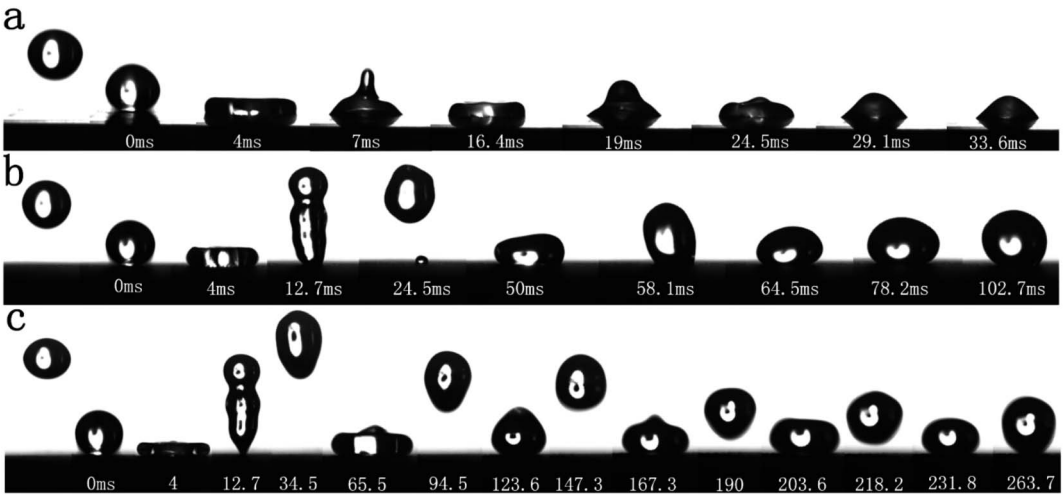

Fig. 7 Bounce behavior of water droplets on the sample surface: (a) smooth Al alloy surface, (b) laser scanning surface with 200 μm pitch, and (c) laser scanning surface with 10 μm pitch.

high-speed camera to record the bounce process of the water droplets when they dropped from the same height on a smooth Al alloy and the laser inscription pitch was 10 μm and 200 μm. The volume of a droplet was 10 μL, the initial speed was 0 mm s^{-1}, and free fall motion was performed. The test results indicated that when water droplets hit different machined surfaces at the same speed, three phenomena were observed: no bounce, partial bounce and bounce back. Specifically, when a water droplet fell on a smooth Al alloy surface, no bounce was found because the surface energy was greater than the cohesive energy of the water droplet. However, when it drops on the surface of the sample with a laser marking distance of 200 μm and 10 μm, one bounce and multiple bounces occur respectively.

Since the initial speed and volume of the water drop were unchanged during the bounce process, the reaction force was the same when they hit the solid surface from the same height. Therefore, whether the water drop can bounce up when it hit the sample depends on the adhesion force of the water drop on the surface of the sample. The surface of the smooth Al alloy was relatively flat, and the water droplets on the surface of the sample were subjected to greater adhesion and did not bounce. Unlike the surface of the smooth Al alloy, the surface of the sample with high static CA had relatively rough micro-nano structures. The three-phase contact line of the contact surface between the water drop and the sample surface was small, so the water drop was affected by the smaller adhesion force of the sample during the spreading and shrinking process. The reaction force overcame the water droplet's gravity and adhesion force to make the water drop bounce. Moreover, the higher the water droplet bounced, the smaller the adhesion force. In Fig. 7b and c, we can find that although water droplets had high static CA on the surface of the sample with a writing pitch of 10 μm and 200 μm, however, the water drop only bounced once on the surface of the sample with an inscription pitch of 200 μm, while it can bounce multiple times when the distance was 10 μm. Besides, the water droplet could still bounce when dripping from a lower position, indicating that the sample surface had a lower adhesion force.

3.5 Surface stability analysis

We separately tested the static CA of the sample surface with time and the chemical stability of the sample surface. Fig. 8a and b is a graph showing the change in CA of the surface of samples with different scribe line spacings within 100 days. The experiment found that the Al alloy surface written by nanosecond fiber laser showed hydrophilic behavior directly after preparation, and the samples with different writing distances after heating treatment showed different wettability behaviors. When the line spacing was 10 μm, the sample still exhibited super-hydrophilicity after heating. When the water droplets touch the sample, it was instantly adsorbed on the surface and spread rapidly. After 10 days of storage at room temperature, the static CA of the sample surface began to increase rapidly. When placed for 30 days, the static CA of the water droplets on the surface of the sample was 129 ± 1.5°, and the contact changed from hydrophilic to hydrophobic state. As time went on, the maximum CA of the surface finally stabilized at 153° ± 1.7°. Similarly, when the distance was 50 μm, the heated sample turned from the super-hydrophilic surface after laser processing to a hydrophobic surface. After the sample was placed in the air for a period of time, the static CA of the surface gradually increased and finally reached 155° ± 1.2°. Fig. 8b illustrates the relationship between the CA of the sample surface with time when the laser scribe line spacing was 100 μm, 150 μm, and 200 μm. Compared with Fig. 8a, it can be observed that when the line spacing was large, the sample directly showed a higher CA after heat treatment, and the surface CA failed to change significantly with time.

Fig. 9 is a graph of the relationship between the CA of the sample surface and the pH when the scanning pitch was 10 μm and 200 μm respectively. To test the chemical stability of the surface of the prepared sample, we mixed 0.1 mol L^{-1} HCl and

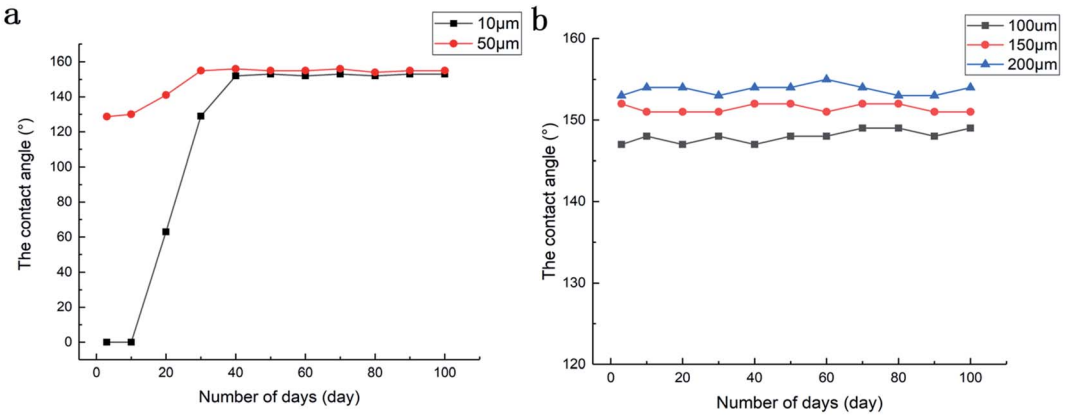

Fig. 8 Relationship of CA of sample surface with time: (a) scanning interval of 10 μm and 50 μm and (b) scanning interval of 100 μm, 150 μm, and 200 μm.

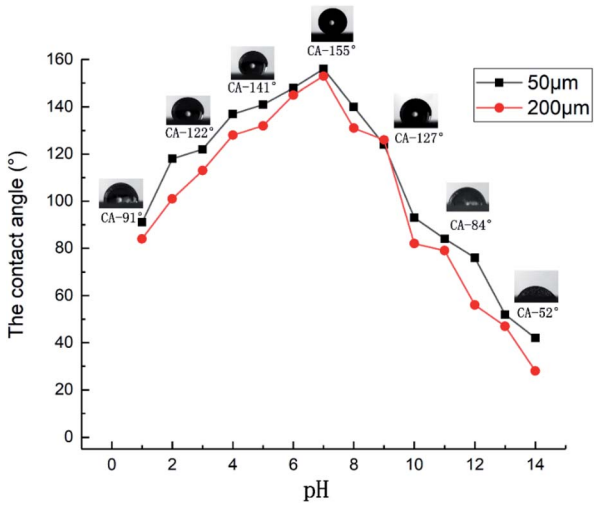

Fig. 9 Relationship between CA and pH.

0.1 mol L^{-1} NaOH solution with different volumes of distilled water to prepare solutions with different pH values. The sample was immersed in solutions of different pH values for 1.5 hours. Then, it was taken out and cleaned ultrasonically for 10 minutes. After drying, the surface CA was tested to determine the chemical stability of the surface. It was observed that the surface wetting of the sample was greatly affected by pH values, and the surface CA first increased and then decreased with the increase in the pH value. As a matter of fact, the minimum CA appeared at the maximum concentration of the solution on both sides, and the alkaline solution had a greater effect on surface wetting. The reason is presumably that alumina is a typical amphoteric oxide. When the sample was placed in a hydrochloric acid/sodium hydroxide solution, the Al oxide film on the surface undergoes a chemical reaction:

The chemical equation of reaction between Al_2O_3 and HCl solutions is as follows:

$$Al_2O_3 + 6HCl = 2AlCl_3 + 3H_2O$$

Ion equation:

$$Al_2O_3+6H^+ = 2Al_3^+ + 3H_2O$$

The chemical equation of reaction between Al_2O_3 and NaOH solutions is as follows:

$$Al_2O_3 + 2NaOH = 2NaAlO_2 + H_2O$$

Ionic equation:

$$Al_2O_3 + 2OH^- = 2Al^- + H_2O$$

The rough micro–nano structure on the surface of the sample was damaged by corrosion, and at the same time, new substances generated by the chemical reaction adhere to the surface of the Al alloy. The change in the substance will also affect the hydrophobicity of the sample surface. As the solution concentration increased, the microstructure of the Al alloy surface was damaged more severely, and the minimum CA on both sides occurred at the strongest acid/alkaline position.

4 Conclusions

All in all, this article mainly studied the rapid preparation of superhydrophobic structures with controllable adhesion and wettability on the surface of the Al alloy treated with EDM. After EDM treatment, the static CA of the Al alloy surface reached 130°, and the water droplets showed high adhesion on the surface. Using a laser to directly process the surface and change the writing pitch, the surface of the sample had a different topography and was accompanied by changes in wettability and adhesion: when the scanning distance was 10 μm, the sample showed super-hydrophilicity after heating. The surface was entirely composed of re-stacked microstructures of the Al alloy melted at high temperature after laser processing. After being

placed in the air for a period of time, the surface had a high static CA, and the water droplets exhibited low adhesion on the surface. When the scanning distance was 50 μm, the surface structure changed from grooves to pits. After heating the sample in air for a period of time, the surface changed from hydrophobic to superhydrophobic state, and the water droplets showed low adhesion on the surface. When the writing pitch was 100 μm, 150 μm, and 200 μm, the EDM area of the sample surface increased with the increase in the laser writing pitch. After heating, the sample immediately showed a high static CA and the water droplets had high adhesion on the surface. The sample was placed in the air for a period of time, and there was no obvious change in the surface wetting state. The surface adhesion and wettability were controllable by regulating laser processing parameters and the proportion of laser and EDM processing area according to the actual requirements, which was of great significance to promote the large-area application of Al alloys in the industry.

Conflicts of interest

No conflict of interest exits in the submission of this manuscript, and manuscript is approved by all authors for publication.

Acknowledgements

All support is greatly acknowledged and appreciated, especially the constructive discussion and criticism from colleagues. Thanks are due to Project supported by the National Natural Science Foundation of China (Grant No. 51705033. U19A200125), the Education Department of Jilin Province (Grant No. JJKH20190560KJ), the Science and Technology Department of Jilin province (Grant No. 20190103001JH and 20180101324) provide financial support for this article.

References

1 Y. T. Cheng, D. E. Rodak, C. A. Wong, *et al.*, Effects of Micro- and Nano-Structures on the Self-Cleaning Behaviour of Lotus Leaves, *Nanotechnology*, 2006, **17**(5), 1359.
2 W. B. Neinhuis, Purity of the sacred lotus, or escape from contamination in biological surfaces, *Planta*, 1997, **202**(1), 1–8.
3 S. Choo, H. J. Choi and H. Lee, Replication of rose-petal surface structure using UV-nanoimprint lithography, *Mater. Lett.*, 2014, **121**, 170–173.
4 L. Feng, Y. Zhang, J. Xi, *et al.*, Petal Effect:? A Superhydrophobic State with High Adhesive Force, *Langmuir*, 2008, **24**(8), 4114–4119.
5 Qian, C. Guang-hua, F. Yan and R. Lu-quan, Super-hydrophobic characteristics of butterfly wing surface, *Journal of Bionic Engineering*, 2004, **1**(4), 249–255.
6 K. Liu and L. Jiang, Bio-inspired design of multiscale structures for function integration, *Nano Today*, 2011, **6**(2), 155–175.
7 Y. L. Wan, J. Lou, Z. J. Yu, *et al.*, Single-step fabrication of bionic-superhydrophobic surface using reciprocating-type high-speed wire cut electrical discharge machining, *Science Bulletin*, 2014, **59**(28), 3691.
8 L. Feng, S. H. Li, Y. Li, *et al.*, Super-Hydrophobic Surfaces: From Natural to Artificial, *ChemInform*, 2003, **14**(24), 1857–1860.
9 R. Evershed, R. Berstan, F. Grew, *et al.*, Water-repellent legs of water striders, *Carbohydr. Res.*, 1983, **113**, 291–299.
10 X. Q. Feng, X. Gao, Z. Wu, *et al.*, Superior Water Repellency of Water Strider Legs with Hierarchical Structures:? Experiments and Analysis, *Langmuir*, 2007, **23**(9), 4892–4896.
11 Y. Lee, Y. Yoo, J. Kim, S. Widhiarini, B. Park, H. C. Park, K. J. Yoon and D. Byun, Mimicking a Superhydrophobic Insect Wing by Argon and Oxygen Ion Beam Treatment on Polytetrafluoroethylene Film, *J. Bionic Eng.*, 2009, **6**(04), 365–370.
12 M. Sun, G. S. Watson, Y. Zheng, *et al.*, Wetting properties on nanostructured surfaces of cicada wings, *J. Exp. Biol.*, 2009, **212**(19), 3148–3155.
13 W. Xiaojun, C. Qian, Z. Jianjun and W. &Yanling, Multivariate coupling mechanism of noctuidae moth wings' surface superhydrophobicity, *Chin. Sci. Bull.*, 2009, (04), 53–59.
14 GangSuna and F. Yan, The Relationship between Superhydrophobicity, Self-Cleaning Performance and Microstructure of Moth Wing, *Appl. Mech. Mater.*, 2015, **727–728**, 273–276.
15 Liu, J. Du, J. Wu and L. Jiang, Superhydrophobic gecko feet with high adhesive forces towards water and their bio-inspired materials, *Nanoscale*, 2011, **4**(3), 768–772.
16 Liu, Y. Zheng, J. Zhai and L. Jiang, Bioinspired super-antiwetting interfaces with special liquid-solid adhesion, *Acc. Chem. Res.*, 2009, **43**(3), 368–377.
17 H. M. S. Hu, G. S. Watson, B. W. Cribb, *et al.*, Non-wetting wings and legs of the cranefly aided by fine structures of the cuticle, *J. Exp. Biol.*, 2011, **214**(6), 915–920.
18 Ding, T. Xiang, Li Cheng, S. Zheng and &W. Chan, Fabrication of self-cleaning super-hydrophobic nickel/graphene hybrid film with improved corrosion resistance on mild steel, *Mater. Des.*, 2016, **117**, 280–288.
19 G. He, S. Lu, W. Xu, *et al.*, Stable superhydrophobic Zn/ZnO surfaces fabricated via electrodeposition on tin substrate for self-cleaning behavior and switchable wettability, *J. Alloys Compd.*, 2018, 772–782.
20 R. Rahul, K. Marina, S. Konstantin, *et al.*, Anti-Icing Superhydrophobic Surfaces: Controlling Entropic Molecular Interactions to Design Novel Icephobic Concrete, *Entropy*, 2016, **18**(4), 132.
21 Y. Liu, X. Li, J. Jin, *et al.*, Anti-icing property of bio-inspired micro-structure superhydrophobic surfaces and heat transfer model, *Appl. Surf. Sci.*, 2017, **400**, 498–505.
22 X. Li, Q. Zhang, Z. Guo, *et al.*, Fabrication of superhydrophobic surface with improved corrosion inhibition on 6061 aluminum alloy substrate, *Appl. Surf. Sci.*, 2015, **342**, 76–83.

23 M.-K. Tang, X.-J. Huang, X.-W. Li, Z.-Y. Huang, S.-M. Zhang and Q.-X. Zhang, Fabrication of superhydrophobic surface with superior anticorrosion and great mechanical stability on aa7075 al alloy via a convenient and efficient approach, *Mater. Express*, 2016, **6**(2), 101–115.

24 V. Priya and S. Soumya, Mohapatra. Durable and regenerable superhydrophobic coatings for brass surfaces with excellent self-cleaning and anti-fogging properties prepared by immersion technique, *Tribol. Int.*, 2018, **123**, 17–25.

25 J. D. Brassard, D. K. Sarkar and J. Perron, Studies of drag on the nanocomposite superhydrophobic surfaces, *Appl. Surf. Sci.*, 2015, **324**, 525–531.

26 C. H. H. Choi and C. J. Kim, Large slip of aqueous liquid flow over a nanoengineered superhydrophobic surface, *Phys. Rev. Lett.*, 2006, **97**(10), 109601–109602.

27 L. Feng, Z. Zhang and Z. Mai, A Super-Hydrophobic and Super-Oleophilic Coating Mesh Film for the Separation of Oil and Water, *Angew. Chem., Int. Ed.*, 2004, **43**(15), 2012–2014.

28 D. Tian, X. Zhang, X. Wang, *et al.*, Micro/nanoscale hierarchical structured ZnO mesh film for separation of water and oil, *Phys. Chem. Chem. Phys.*, 2011, **13**(32), 14606.

29 J. Wu, J. Chen, K. Qasim, *et al.*, A hierarchical mesh film with superhydrophobic and superoleophilic properties for oil and water separation, *J. Chem. Technol. Biotechnol.*, 2012, **87**(3), 427–430.

30 C. H. Xue, J. Chen, W. Yin, *et al.*, Superhydrophobic conductive textiles with antibacterial property by coating fibers with silver nanoparticles, *Appl. Surf. Sci.*, 2012, **258**(7), 2468–2472.

31 M. Shateri-Khalilabad and M. E. Yazdanshenas, Fabrication of superhydrophobic, antibacterial, and ultraviolet-blocking cotton fabric, *J. Text. Inst.*, 2013, **104**(8), 861–869.

32 S. Z. Wu, D. Wu, J. Yao, *et al.*, One-Step Preparation of Regular Micropearl Arrays for Two-Direction Controllable Anisotropic Wetting, *Langmuir*, 2010, **26**(14), 12012–12016.

33 S. Wu, J. Wang, L. Niu, *et al.*, Reversible switching between isotropic and anisotropic wetting by one-direction curvature tuning on flexible superhydrophobic surfaces, *Appl. Phys. Lett.*, 2011, **98**(8), 081902.

34 J. Sun, K. Hu, X. Liu, *et al.*, Fabrication of superhydrophobic surfaces on copper substrates via flow plating technology, *Micro Nano Lett.*, 2015, **10**(2), 88–92.

35 A. Chaudhary and C. B. Harish, Nanometric Multiscale Rough CuO/Cu(OH)2 Superhydrophobic Surfaces Prepared by a Facile One-Step Solution-Immersion Process: Transition to Superhydrophilicity with Oxygen Plasma Treatment, *J. Phys. Chem. C*, 2011, **115**, 18213–18220.

36 A. V. Rao, S. S. Latthe, S. A. Mahadik, *et al.*, Mechanically stable and corrosion resistant superhydrophobic sol–gel coatings on copper substrate, *Appl. Surf. Sci.*, 2011, **257**(13), 5772–5776.

37 Z. Duan, Z. Zhao, D. Luo, *et al.*, A facial approach combining photosensitive sol–gel with self-assembly method to fabricate superhydrophobic TiO2 films with patterned surface structure, *Appl. Surf. Sci.*, 2016, **360**, 1030–1035.

38 Z. Lian, J. Xu and Z. Wang, Biomimetic Superlyophobic Metallic Surfaces Focusing on Their Fabrication and Applications, *J. Bionic Eng.*, 2020, **17**(8), 1–33.

39 Y. Liu, X. Yin, J. Zhang, *et al.*, Biomimetic hydrophobic surface fabricated by chemical etching method from hierarchically structured magnesium alloy substrate, *Appl. Surf. Sci.*, 2013, **280**, 845–849.

40 L. Zhong, D. W. Gong, J. Y. Long, D. F. Jiang, P. X. Fan and H. J. Zhang, Robust and stable transparent superhydrophobic poly-dimethylsiloxane films by duplicating via femtosecond laser ablated template, *ACS Appl. Mater. Interfaces*, 2016, **8**, 17511–17518.

41 J. Wang, L. Gao, Y. Li, *et al.*, Experimental research on laser interference micro/nano fabrication of hydrophobic modification of stent surface, *Lasers in Medical Science*, 2016, **32**(1), 1–7.

42 L. Zhong, D. W. Gong, J. Y. Long, D. F. Jiang, P. X. Fan and H. J. Zhang, Robust and stable transparent superhydrophobic poly-dimethylsiloxane films by duplicating via femtosecond laser ablated template, *ACS Appl. Mater. Interfaces*, 2016, **8**, 17511–17518.

43 Jagdheesh, M. Diaz and J. L. Ocana, Bio inspired self–cleaning ultrahydrophobicaluminium surface by laser processing, *RSC Adv.*, 2016, **6**, 72933–72941.

44 J. Li, Y. Zhou, F. Fan, F. Du and H. Yu, Controlling surface wettability and adhesive properties by laser marking approach, *Opt. Laser Technol.*, 2019, **115**, 160–165.